12-29-2014

Computational Approaches for Generating Electromagnetic Gaussian Schell-model Sources

Santasri Basu
Air Force Institute of Technology

Milo W. Hyde IV
Air Force Institute of Technology

Xifeng Xiao
New Mexico State University

David G. Voelz
Air Force Institute of Technology

Olga Korotkova
University of Miami

Recommended Citation

Santasri Basu, Milo W. Hyde, Xifeng Xiao, David G. Voelz, and Olga Korotkova, "Computational approaches for generating electromagnetic Gaussian Schell-model sources," Opt. Express 22, 31691-31707 (2014). https://doi.org/10.1364/OE.22.031691

Computational approaches for generating electromagnetic Gaussian Schell-model sources

Santasri Basu,[1,2,*] Milo W. Hyde IV,[1] Xifeng Xiao,[3] David G. Voelz,[3] and Olga Korotkova[4]

[1]*Air Force Institute of Technology, 2950 Hobson Way, Dayton, OH 45433, USA*
[2]*Oak Ridge Institute for Science and Education, 1299 Bethel Valley Road, Oak Ridge, TN 37380, USA*
[3]*Klipsch School of Electrical and Computer Engineering, New Mexico State University, Las Cruces, NM 88003, USA*
[4]*Department of Physics, University of Miami, Coral Gables, FL 33146, USA*
[*]*santasri.basu@afit.edu*

Abstract: Two different methodologies for generating an electromagnetic Gaussian-Schell model source are discussed. One approach uses a sequence of random phase screens at the source plane and the other uses a sequence of random complex transmittance screens. The relationships between the screen parameters and the desired electromagnetic Gaussian-Schell model source parameters are derived. The approaches are verified by comparing numerical simulation results with published theory. This work enables one to design an electromagnetic Gaussian-Schell model source with pre-defined characteristics for wave optics simulations or laboratory experiments.

OCIS codes: (030.0030) Coherence and statistical optics; (030.1670) Coherent optical effects; (110.4980) Partial coherence in imaging; (260.5430) Polarization.

References and links

1. D. F. James, "Change of polarization of light beams on propagation in free space," J. Opt. Soc. Am. A **11**(5), 1641–1649 (1994).
2. F. Gori, M. Santarsiero, G. Piquero, R. Borghi, A. Mondello, and R. Simon, "Partially polarized Gaussian Schell-model beams," J. Opt. A, Pure Appl. Opt. **3**(1), 1–9 (2001).
3. S. Zhu, Y. Cai, and O. Korotkova, "Propagation factor of a stochastic electromagnetic Gaussian Schell-model beam," Opt. Express **18**(12), 12587–12598 (2010).
4. J. C. G. de Sande, G. Piquero, M. Santarsiero, and F. Gori, "Partially coherent electromagnetic beams propagating through double-wedge depolarizers," J. Opt. **16**(3), 035708 (2014).
5. Y. Zhu, D. Zhao, and X. Du, "Propagation of stochastic Gaussian-Schell model array beams in turbulent atmosphere," Opt. Express **16**(22), 18437–18442 (2008).
6. O. Korotkova, M. Salem, and E. Wolf, "The far-zone behavior of the degree of polarization of electromagnetic beams propagating through atmospheric turbulence," Opt. Commun. **233**(4-6), 225–230 (2004).
7. M. Salem, O. Korotkova, A. Dogariu, and E. Wolf, "Polarization changes in partially coherent electromagnetic beams propagating through turbulent atmosphere," Waves Random Media **14**(4), 513–523 (2004).
8. O. Korotkova, "Scintillation index of a stochastic electromagnetic beam propagating in random media," Opt. Commun. **281**(9), 2342–2348 (2008).
9. O. Korotkova, *Random Beams: Theory and Applications* (CRC, 2013).
10. E. Wolf, *Introduction to the Theory of Coherence and Polarization of Light* (Cambridge, 2007).
11. F. Gori, "Matrix treatment for partially polarized, partially coherent beams," Opt. Lett. **23**(4), 241–243 (1998).
12. O. Korotkova, M. Salem, and E. Wolf, "Beam conditions for radiation generated by an electromagnetic Gaussian Schell-model source," Opt. Lett. **29**(11), 1173–1175 (2004).
13. J. Tervo, T. Setälä, and A. T. Friberg, "Theory of partially coherent electromagnetic fields in the space-frequency domain," J. Opt. Soc. Am. A **21**(11), 2205–2215 (2004).
14. H. Roychowdhury and O. Korotkova, "Realizability conditions for electromagnetic Gaussian Schell-model sources," Opt. Commun. **249**(4-6), 379–385 (2005).
15. F. Gori, M. Santarsiero, R. Borghi, and V. Ramirez-Sanchez, "Realizability condition for electromagnetic Schell-model souces," J. Opt. Soc. Am. A **25**(5), 1016–1021 (2008).
16. A. S. Ostrovsky, G. Martínez-Niconoff, V. Arrizón, P. Martínez-Vara, M. A. Olvera-Santamaría, and C. Rickenstorff-Parrao, "Modulation of coherence and polarization using liquid crystal spatial light modulators," Opt. Express **17**(7), 5257–5264 (2009).

#225412 - $15.00 USD Received 21 Oct 2014; revised 21 Nov 2014; accepted 25 Nov 2014; published 15 Dec 2014

17. X. Xiao and D. Voelz, "Wave optics simulation of partially coherent and partially polarized beam propagation in turbulence," Proc. SPIE **7464**, 74640T (2009).
18. G. Piquero, F. Gori, P. Romanini, M. Santarsiero, R. Borghi, and A. Mondello, "Synthesis of partially polarized Gaussian Schell-model sources," Opt. Commun. **208**(1-3), 9–16 (2002).
19. F. Wang, G. Wu, X. Liu, S. Zhu, and Y. Cai, "Experimental measurement of the beam parameters of an electromagnetic Gaussian Schell-model source," Opt. Lett. **36**(14), 2722–2724 (2011).
20. T. Shirai, O. Korotkova, and E. Wolf, "A method of generating electromagnetic Gaussian Schell-model beams," J. Opt. A, Pure Appl. Opt. **7**(5), 232–237 (2005).
21. A. S. Ostrovsky, G. Rodríguez-Zurita, C. Meneses-Fabián, M. A. Olvera-Santamaría, and C. Rickenstorff-Parrao, "Experimental generating the partially coherent and partially polarized electromagnetic source," Opt. Express **18**(12), 12864–12871 (2010).
22. P. Meemon, M. Salem, K. S. Lee, M. Chopra, and J. P. Rolland, "Determination of the coherency matrix of a broadband stochastic electromagnetic light beam," J. Mod. Opt. **55**(17), 2765–2776 (2008).
23. S. Avramov-Zamurovic, C. Nelson, R. Malek-Madani, and O. Korotkova, "Polarization-induced reduction in scintillation of optical beams propagating in simulated turbulent atmospheric channels," Waves Complex Random Media. in press.
24. S. Avramov-Zamurovic, C. Nelson, R. Malek-Madani, and O. Korotkova, "The dependence of the intensity PDF of a random beam propagating in the maritime atmosphere on source coherence," Waves Complex Random Media **24**(1), 69–82 (2014).
25. J. W. Goodman, *Statistical Optics* (Wiley, 2000).
26. Boulder Nonlinear Systems, Inc., *Spatial Light Modulators—XY Series* (Retrieved November 13, 2014 from *http://www.meadowlark.com/store/data_sheet/Datasheet_XYseries_SLM.pdf*).
27. S. Sahin, Z. Tong, and O. Korotkova, "Sensing of semi-rough targets embedded in atmospheric turbulence by means of stochastic electromagnetic beams," Opt. Commun. **283**(22), 4512–4518 (2010).

1. Introduction

The electromagnetic Gaussian Schell-model (EGSM) source/beam was introduced as an extension of the scalar Gaussian Schell-model (GSM) beam [1, 2]. Since then, it has attracted special attention due to the interesting polarization evolution that can occur on its propagation and the reduction in scintillation that is possible in free-space optical communications, imaging through turbulence, and remote sensing applications [3–10]. The ability to customize the EGSM attributes can lead to improved performance for particular applications and scenarios.

An EGSM beam can be described by a 2 × 2 cross-spectral density (CSD) matrix that characterizes second-order correlations between two mutually orthogonal components of the fluctuating electric field at a pair of spatial arguments and frequency [10]. Substantial progress has been made on the theoretical understanding of these beams including their propagation aspects, correlation features, and realizability conditions [11–15]. Concurrently, various methods have been proposed to produce EGSM sources numerically and experimentally [16–23]. These efforts include an approach to experimentally synthesize EGSM sources with the same mutually orthogonal electric field components [18], an experimental measurement to verify the validity of the EGSM beam parameters [19, 22], and a practical method of producing a general EGSM source [20]. Most recently, a reduction in scintillation for a particular subclass of EGSM beam (completely unpolarized) was successfully demonstrated for propagation in thermally simulated atmospheric turbulence [23]. These studies provide practical techniques to physically realize the EGSM beam and successfully validate the existing theory; however, a practical ability to design and control the EGSM beam characteristics was not the primary emphasis of these efforts.

In this paper, the fundamental relationships between the two orthogonal polarization components of an EGSM beam are examined and a computational approach for creating numerical random screens that are associated with the components is presented. The desired EGSM beam parameters determine the selection of the screen parameters. The concept is that a pair of such screens is applied at the source plane to two orthogonally polarized coherent waves. The two resulting wave components constitute an instantaneous electromagnetic beam realization. Sufficiently large, mutually independent sequences of the screen pairs are then applied and the resulting intensities for each field component are averaged over these ensembles of realizations. The four average intensities, two representing self-correlations and

#225412 - $15.00 USD Received 21 Oct 2014; revised 21 Nov 2014; accepted 25 Nov 2014; published 15 Dec 2014

two representing joint correlations, between the two components comprise the EGSM beam. The beams produced in this manner are consistent with the EGSM realizability conditions stemming from the fundamental properties of the CSD matrix [14, 15]. The produced ensembles of screens can be used in a numerical wave optics simulation or in the laboratory with spatial light modulators (SLMs).

In Section 2, two screen methodologies, the phase screen (PS) and the complex transmittance screen (CS), are introduced. The relationships between the screen parameters and the desired EGSM beam parameters are explored and the benefits and constraints of the two approaches are discussed. The screen methodologies are validated in Section 3 via numerical modeling of typical EGSM beams and comparison of the results with theoretical predictions. Some final remarks and future research directions are given in Section 4.

2. Methodology

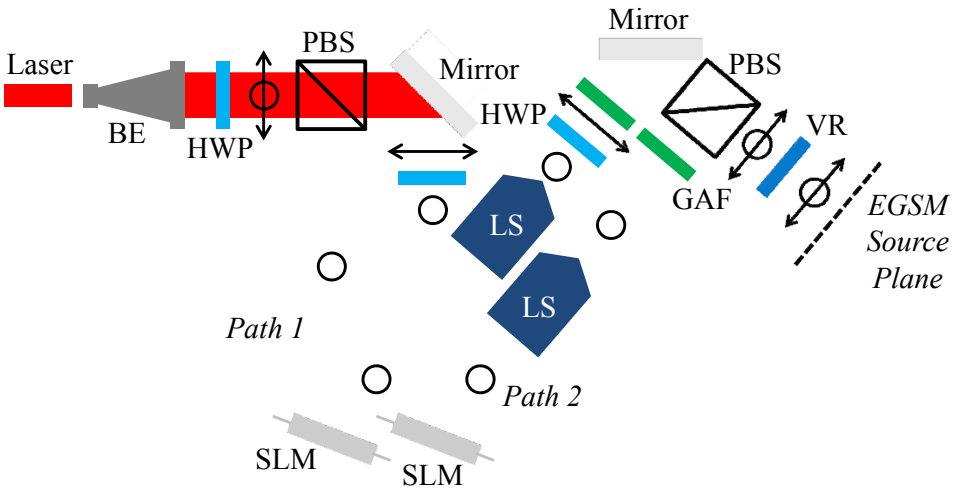

Fig. 1. Proposed experimental schematic for generating EGSM sources. The acronyms used in the figure are beam expander (BE), half-wave plate (HWP), polarizing beamsplitter (PBS), lens systems (LS), spatial light modulator (SLM), Gaussian amplitude filter (GAF), and variable retarder (VR). The polarization state of the light passing through the system is denoted by two-sided arrows (representing horizontal polarization) and circles (representing vertical polarization). When both are present, the light is in a general polarization state, i.e., polarized, partially polarized, or unpolarized.

Figure 1 shows a proposed experimental schematic for generating EGSM sources. Note that this proposed set-up is similar to that presented in Ref [20]. Light leaves a laser and traverses a beam expander (BE) and half-wave plate (HWP) before being split along two paths by a polarizing beam splitter (PBS). The initial HWP is used to control the relative amplitudes of the fields along each path. In paths 1 and 2, the light is polarized vertically (denoted by the circle) and horizontally (denoted by the two-sided arrow), respectively. It is assumed here that the SLMs control only vertically polarized light; thus, a HWP is used in path 2 to transform horizontal linear polarization into vertical polarization.

The light in both paths is then incident on the SLMs. Because of their widespread use, it is assumed that the SLMs in Fig. 1 are reflective, phase-only SLMs. The SLMs impart random, correlated phases to the light in paths 1 and 2. After the SLMs, the light enters general lens systems (LS). These LS could be spatial filters, 4-*f* systems, etc. and are included to remove unwanted diffraction orders, produced by the SLMs, which may corrupt the desired EGSM source output.

#225412 - $15.00 USD Received 21 Oct 2014; revised 21 Nov 2014; accepted 25 Nov 2014; published 15 Dec 2014

After traversing the LS, the light in both paths passes through Gaussian amplitude filters (GAFs) which set the desired Gaussian amplitude widths of the EGSM source (discussed in more detail below). The light from path 1 and path 2 is then recombined using a PBS. Note that the HWP, located before the GAF, on path 1 is required to transform the polarization state from vertical to horizontal polarization so that the light from both paths can be recombined. Lastly, a liquid crystal variable retarder (VR) is included to control the relative phasing between the vertical and horizontal polarization states.

It must be stated that the experimental set-up depicted in Fig. 1 is hypothetical. No experimental results are presented in this paper. The approaches presented here for generating EGSM sources are validated via simulation. The above description is included to provide background on how one might generate EGSM sources in practice. An experimental system similar to the one in Fig. 1 is currently in work. Experimental results will be presented in a future paper.

Two methods for generating EGSM sources are presented in this paper—the PS and CS methods. The PS approach involves generating two random phase screens, one for each polarization component. This approach can be implemented in the laboratory with two phase-only SLMs as shown in Fig. 1. The interested reader is referred to Ref [24]. for the practical aspects of generating a scalar GSM beam with a single nematic phase-only SLM. The PS approach is equivalent to that presented in Ref [20]; however, here, the derivation is presented differently.

While the PS approach is useful for practical implementation purposes, its main disadvantage is that the autocorrelation function of the screen transmittances is typically not of the desired form. This is a significant problem when the desired autocorrelation function is not Gaussian. The CS approach, on the other hand, does not suffer from this shortcoming. This approach involves generating two screens with complex transmittance functions, i.e., both the amplitude and phase of the incident wave are randomized spatially upon transmission through the screen. The CS approach is ideal for numerical simulations, but laboratory implementation is rather difficult because both the amplitude and phase of the source must be controlled.

The elements of the CSD matrix of an EGSM source are [10]

$$\begin{aligned} W_{\alpha\beta}\left(\boldsymbol{\rho}_1,\boldsymbol{\rho}_2,0;\omega\right) &= \sqrt{S_\alpha\left(\boldsymbol{\rho}_1;\omega\right)}\sqrt{S_\beta\left(\boldsymbol{\rho}_2;\omega\right)}\mu_{\alpha\beta}\left(\left|\boldsymbol{\rho}_1-\boldsymbol{\rho}_2\right|;\omega\right) \\ S_\alpha\left(\boldsymbol{\rho};\omega\right) &= A_\alpha^2\exp\left(\frac{-\rho^2}{2\sigma_\alpha^2}\right) \\ \mu_{\alpha\beta}\left(\left|\boldsymbol{\rho}_1-\boldsymbol{\rho}_2\right|;\omega\right) &= B_{\alpha\beta}\exp\left(\frac{-\left|\boldsymbol{\rho}_1-\boldsymbol{\rho}_2\right|^2}{2\delta_{\alpha\beta}^2}\right), \end{aligned} \tag{1}$$

where $\alpha,\beta = x,y$, S_α is the spectral density, $\mu_{\alpha\beta}$ is the spectral correlation function and $\boldsymbol{\rho} = \hat{\boldsymbol{x}}x + \hat{\boldsymbol{y}}y$. Further, σ_α and $\delta_{\alpha\beta}$ are the r.m.s. widths of the spectral density and correlation profiles, respectively. The parameters σ_α, $B_{\alpha\beta}$, and $\delta_{\alpha\beta}$ are constrained by the following relationships:

#225412 - $15.00 USD Received 21 Oct 2014; revised 21 Nov 2014; accepted 25 Nov 2014; published 15 Dec 2014

$$
\begin{aligned}
B_{\alpha\beta} &= 1 \quad \alpha = \beta \\
\left|B_{\alpha\beta}\right| &\le 1 \quad \alpha \ne \beta \\
B_{\alpha\beta} &= B_{\beta\alpha}^{*} \\
\delta_{\alpha\beta} &= \delta_{\beta\alpha} \\
\frac{1}{4\sigma_{\alpha}^{2}} + \frac{1}{\delta_{\alpha\alpha}^{2}} &\ll \frac{2\pi^{2}}{\lambda^{2}}.
\end{aligned}
\tag{2}
$$

In addition, an EGSM source must satisfy the fork inequality

$$
\sqrt{\frac{\delta_{xx}^{2} + \delta_{yy}^{2}}{2}} \le \delta_{xy} \le \sqrt{\frac{\delta_{xx}\delta_{yy}}{\left|B_{xy}\right|}}
\tag{3}
$$

to be realizable [15]. It is imperative to show that both proposed approaches produce sources whose parameters obey the above constraints. Hereafter, the dependence on the radian frequency ω is omitted for the sake of brevity.

2.1 PS approach

Let the electric field in the source plane, $z = 0$, be

$$
\begin{aligned}
\boldsymbol{E}(\boldsymbol{\rho}, 0) &= \hat{\mathbf{x}} E_{x}(\boldsymbol{\rho}) + \hat{\mathbf{y}} E_{y}(\boldsymbol{\rho}) \\
E_{\alpha}(\boldsymbol{\rho}) &= C_{\alpha} \exp\left(\frac{-\rho^{2}}{4\sigma_{\alpha}^{2}}\right) \exp\left[\mathrm{j}\phi_{\alpha}(\boldsymbol{\rho})\right],
\end{aligned}
\tag{4}
$$

where $C_{\alpha} = \left|C_{\alpha}\right| \exp(\mathrm{j}\theta_{\alpha})$ is a complex constant and $\phi_{\alpha}(\boldsymbol{\rho})$ is the random phase contribution due to the screen. Performing the autocorrelations necessary to fill the CSD matrix produces

$$
\begin{aligned}
\left\langle \boldsymbol{E}(\boldsymbol{\rho}_{1}, 0) \boldsymbol{E}^{*}(\boldsymbol{\rho}_{2}, 0) \right\rangle &= \mathbf{W}(\boldsymbol{\rho}_{1}, \boldsymbol{\rho}_{2}, 0) = \begin{bmatrix} \left\langle E_{x}(\boldsymbol{\rho}_{1}, 0) E_{x}^{*}(\boldsymbol{\rho}_{2}, 0) \right\rangle & \left\langle E_{x}(\boldsymbol{\rho}_{1}, 0) E_{y}^{*}(\boldsymbol{\rho}_{2}, 0) \right\rangle \\ \left\langle E_{y}(\boldsymbol{\rho}_{1}, 0) E_{x}^{*}(\boldsymbol{\rho}_{2}, 0) \right\rangle & \left\langle E_{y}(\boldsymbol{\rho}_{1}, 0) E_{y}^{*}(\boldsymbol{\rho}_{2}, 0) \right\rangle \end{bmatrix} \\
\left\langle E_{\alpha}(\boldsymbol{\rho}_{1}, 0) E_{\beta}^{*}(\boldsymbol{\rho}_{2}, 0) \right\rangle &= C_{\alpha} C_{\beta}^{*} \exp\left[-\left(\frac{\rho_{1}^{2}}{4\sigma_{\alpha}^{2}} + \frac{\rho_{2}^{2}}{4\sigma_{\beta}^{2}} \right) \right] \left\langle \exp\left[\mathrm{j}\phi_{\alpha}(\boldsymbol{\rho}_{1})\right] \exp\left[-\mathrm{j}\phi_{\beta}(\boldsymbol{\rho}_{2})\right] \right\rangle.
\end{aligned}
\tag{5}
$$

The phase screen realizations are sample functions drawn from two correlated Gaussian random processes. Hereafter, for the sake of brevity, functions evaluated at $\boldsymbol{\rho}_{1}$ or $\boldsymbol{\rho}_{2}$ are denoted with a subscript 1 or 2, respectively. For example, $\phi_{\alpha}(\boldsymbol{\rho}_{1})$ is expressed as $\phi_{\alpha 1}$.

The expectation on the second line of Eq. (5) is recognized as the joint characteristic function of the Gaussian random variables ϕ_{α} and ϕ_{β} evaluated at $\omega_{1} = 1$ and $\omega_{2} = -1$, where ω_{1} and ω_{2} are radian frequencies. This expression is [25]

$$
\left\langle \exp\left[\mathrm{j}\phi_{\alpha 1}\right] \exp\left[-\mathrm{j}\phi_{\beta 2}\right] \right\rangle = \exp\left\{ -\frac{1}{2}\left(\sigma_{\phi_{\alpha}}^{2} + \sigma_{\phi_{\beta}}^{2}\right) \left[1 - \frac{2\sigma_{\phi_{\alpha}}\sigma_{\phi_{\beta}}}{\sigma_{\phi_{\alpha}}^{2} + \sigma_{\phi_{\beta}}^{2}} \rho_{\phi_{\alpha}\phi_{\beta}} \gamma_{\phi_{\alpha}\phi_{\beta}}\left(\left|\boldsymbol{\rho}_{1} - \boldsymbol{\rho}_{2}\right|; \ell_{\phi_{\alpha}\phi_{\beta}} \right) \right] \right\},
\tag{6}
$$

#225412 - $15.00 USD Received 21 Oct 2014; revised 21 Nov 2014; accepted 25 Nov 2014; published 15 Dec 2014

where σ_{ϕ_α} and σ_{ϕ_β} are the standard deviations of the ϕ_α and ϕ_β phase screens, respectively; $0 \le \rho_{\phi_\alpha\phi_\beta} \le 1$ is a correlation coefficient ($\rho_{\phi_\alpha\phi_\beta} = 1$ if $\alpha = \beta$); and $\gamma_{\phi_\alpha\phi_\beta}$ is the normalized cross-correlation function taken here to be Gaussian-shaped, viz.,

$$\gamma_{\phi_\alpha\phi_\beta}\left(\left|\boldsymbol{\rho}_1 - \boldsymbol{\rho}_2\right|; \ell_{\phi_\alpha\phi_\beta}\right) = \exp\left(-\frac{\left|\boldsymbol{\rho}_1 - \boldsymbol{\rho}_2\right|^2}{\ell^2_{\phi_\alpha\phi_\beta}}\right). \tag{7}$$

The symbol $\ell_{\phi_\alpha\phi_\beta}$ is the spatial cross-correlation radius of the phase screens ϕ_α and ϕ_β. Assuming that $\left(\sigma^2_{\phi_\alpha} + \sigma^2_{\phi_\beta}\right)\Big/2 \gg 1$, or equivalently $\sigma_{\phi_\alpha}, \sigma_{\phi_\beta} \ge \pi$, $\gamma_{\phi_\alpha\phi_\beta}$ can be safely approximated as $\gamma_{\phi_\alpha\phi_\beta} \approx 1 - \left|\boldsymbol{\rho}_1 - \boldsymbol{\rho}_2\right|^2 \Big/ \ell^2_{\phi_\alpha\phi_\beta}$. Substituting this expression into Eq. (6), then into Eq. (5), and simplifying produces

$$\begin{aligned}\left\langle E_{\alpha 1} E^*_{\beta 2}\right\rangle \approx C_\alpha C^*_\beta \exp\left[-\left(\frac{\rho_1^2}{4\sigma_\alpha^2} + \frac{\rho_2^2}{4\sigma_\beta^2}\right)\right] \exp\left[-\frac{1}{2}\left(\sigma^2_{\phi_\alpha} - 2\rho_{\phi_\alpha\phi_\beta}\sigma_{\phi_\alpha}\sigma_{\phi_\beta} + \sigma^2_{\phi_\beta}\right)\right] \\ \exp\left[-\frac{\left|\boldsymbol{\rho}_1 - \boldsymbol{\rho}_2\right|^2}{\ell^2_{\phi_\alpha\phi_\beta}\Big/\sigma_{\phi_\alpha}\sigma_{\phi_\beta}\rho_{\phi_\alpha\phi_\beta}}\right].\end{aligned} \tag{8}$$

By comparing Eq. (8) to Eq. (1), one deduces the following relationships:

$$\begin{aligned} \delta_{xx} &= \frac{1}{\sqrt{2}}\frac{\ell_{\phi_x\phi_x}}{\sigma_{\phi_x}} & A_x &= \left|C_x\right| \\ \delta_{yy} &= \frac{1}{\sqrt{2}}\frac{\ell_{\phi_y\phi_y}}{\sigma_{\phi_y}} & A_y &= \left|C_y\right| \\ \delta_{xy} &= \frac{1}{\sqrt{2}}\frac{\ell_{\phi_x\phi_y}}{\sqrt{\sigma_{\phi_x}\sigma_{\phi_y}\rho_{\phi_x\phi_y}}} & & \\ \left|B_{xy}\right| &= \exp\left[-\frac{1}{2}\left(\sigma^2_{\phi_x} - 2\rho_{\phi_x\phi_y}\sigma_{\phi_x}\sigma_{\phi_y} + \sigma^2_{\phi_y}\right)\right] & \angle B_{xy} &= \theta_x - \theta_y. \end{aligned} \tag{9}$$

Note that the relations reported in the left column of Eq. (9) are coupled and cannot be chosen at will. On the other hand, the relations in the right column of Eq. (9) are uncoupled and can be chosen at will. Referring back to Fig. 1, A_x and A_y are controlled using the initial HWP, σ_x and σ_y are set by using the appropriate GAFs, and $\angle B_{xy}$ is set using the VR. The remaining EGSM source parameters are determined by the statistical properties of the phases commanded to the SLMs discussed in detail in Section 2.3.

2.2. CS approach

Let the electric field components in the source plane, $z = 0$, be

$$E_\alpha(\boldsymbol{\rho}) = C_\alpha \exp\left(\frac{-\rho^2}{4\sigma_\alpha^2}\right) T_\alpha(\boldsymbol{\rho}), \tag{10}$$

where $T_\alpha(\boldsymbol{\rho})$ is the complex transmittance function of the screen. Performing the autocorrelations necessary to fill the CSD matrix produces

#225412 - $15.00 USD Received 21 Oct 2014; revised 21 Nov 2014; accepted 25 Nov 2014; published 15 Dec 2014

$$\left\langle E_{\alpha 1}E_{\beta 2}^{*}\right\rangle = C_{\alpha}C_{\beta}^{*}\exp\left[-\left(\frac{\rho_1^2}{4\sigma_{\alpha}^2}+\frac{\rho_2^2}{4\sigma_{\beta}^2}\right)\right]\left\langle T_{\alpha 1}T_{\beta 2}^{*}\right\rangle. \tag{11}$$

Just like ϕ_α and ϕ_β in the PS approach, T_α and T_β are sample functions drawn from two correlated Gaussian random processes. This time, however, the random processes are complex.

The expectation in Eq. (11) is recognized as the cross-correlation function of the Gaussian random processes T_α and T_β:

$$\left\langle T_{\alpha 1}T_{\beta 2}^{*}\right\rangle = \sigma_{T_\alpha}\sigma_{T_\beta}\rho_{T_\alpha T_\beta}\gamma_{T_\alpha T_\beta}\left(\left|\boldsymbol{\rho}_1-\boldsymbol{\rho}_2\right|;\ell_{T_\alpha T_\beta}\right), \tag{12}$$

where σ_{T_α} and σ_{T_β} are the standard deviations of the T_α and T_β screens, respectively; $0\le\rho_{T_\alpha T_\beta}\le 1$ is a correlation coefficient ($\rho_{T_\alpha T_\beta}=1$ if $\alpha=\beta$); and $\gamma_{T_\alpha T_\beta}$ is the normalized cross-correlation function taken here to be Gaussian-shaped, namely,

$$\gamma_{T_\alpha T_\beta}\left(\left|\boldsymbol{\rho}_1-\boldsymbol{\rho}_2\right|;\ell_{T_\alpha T_\beta}\right)=\exp\left(-\frac{\left|\boldsymbol{\rho}_1-\boldsymbol{\rho}_2\right|^2}{\ell_{T_\alpha T_\beta}^2}\right). \tag{13}$$

The symbol $\ell_{T_\alpha T_\beta}$ is the spatial cross-correlation radius of the complex transmittance screens T_α and T_β. Substituting Eqs. (12) and (13) into Eq. (11) and simplifying produces

$$\left\langle E_{\alpha 1}E_{\beta 2}^{*}\right\rangle = C_{\alpha}C_{\beta}^{*}\sigma_{T_\alpha}\sigma_{T_\beta}\rho_{T_\alpha T_\beta}\exp\left[-\left(\frac{\rho_1^2}{4\sigma_{\alpha}^2}+\frac{\rho_2^2}{4\sigma_{\beta}^2}\right)\right]\exp\left[-\frac{\left|\boldsymbol{\rho}_1-\boldsymbol{\rho}_2\right|^2}{\ell_{T_\alpha T_\beta}^2}\right]. \tag{14}$$

By comparing Eq. (14) to Eq. (1), the following relationships are deduced:

$$\begin{aligned}
\delta_{xx}&=\frac{\ell_{T_xT_x}}{\sqrt{2}} \qquad A_x=\sigma_{T_x}\left|C_x\right|\\
\delta_{yy}&=\frac{\ell_{T_yT_y}}{\sqrt{2}} \qquad A_y=\sigma_{T_y}\left|C_y\right|\\
\delta_{xy}&=\frac{\ell_{T_xT_y}}{\sqrt{2}}\\
\left|B_{xy}\right|&=\rho_{T_xT_y} \qquad \angle B_{xy}=\theta_x-\theta_y.
\end{aligned} \tag{15}$$

While not yet evident, the relations reported in the left column of Eq. (15) are coupled and cannot be chosen at will. The relations in the right column are uncoupled and can be chosen at will.

2.3. Generating phase screens (PS approach)

In this section, a method for generating the required discretized ϕ_x and ϕ_y is presented. Of the two approaches discussed above, the PS approach is the most applicable to laboratory research because of the commercial availability of phase-only SLMs. The specifications of commercial SLMs (size of active area, number of pixels, pixel pitch, etc.) vary by vendor. Here, the specifications of the Boulder Nonlinear Systems (BNS) Model P512-0635 SLM are adopted, i.e., 512 × 512 pixel array with a $15\,\mu$m pitch [26]. These numbers are used in the simulation results presented in Section 3.

#225412 - $15.00 USD Received 21 Oct 2014; revised 21 Nov 2014; accepted 25 Nov 2014; published 15 Dec 2014

Let ϕ and $\tilde{\phi}$ be Fourier transform pairs, i.e.,

$$\begin{aligned}\tilde{\phi}\left(f_x, f_y\right) &= \int_{-\infty}^{\infty}\int_{-\infty}^{\infty} \phi(x,y)\exp\left(-\mathrm{j}2\pi f_x x\right)\exp\left(-\mathrm{j}2\pi f_y y\right)\mathrm{d}x\mathrm{d}y \\ \phi(x,y) &= \int_{-\infty}^{\infty}\int_{-\infty}^{\infty} \tilde{\phi}\left(f_x, f_y\right)\exp\left(\mathrm{j}2\pi f_x x\right)\exp\left(\mathrm{j}2\pi f_y y\right)\mathrm{d}f_x\mathrm{d}f_y.\end{aligned} \tag{16}$$

Since ϕ_α obeys Gaussian statistics,

$$\begin{aligned}\left\langle \phi_x(x,y)\right\rangle &= \left\langle \phi_y(x,y)\right\rangle = \left\langle \phi_\alpha(x,y)\right\rangle = 0 \\ \left\langle \phi_\alpha(x_1,y_1)\phi_\alpha^*(x_2,y_2)\right\rangle &= \sigma_{\phi_\alpha}^2 \exp\left(-\frac{\left|\boldsymbol{\rho}_1-\boldsymbol{\rho}_2\right|^2}{\ell_{\phi_\alpha\phi_\alpha}^2}\right).\end{aligned} \tag{17}$$

The phase screen ϕ_α is real; the complex conjugate on the second term in the autocorrelation is provided only for completeness.

Expanding ϕ_α in a Fourier series yields

$$\begin{aligned}\phi_\alpha(x,y) &= \mathrm{Re}\left[\sum_{m,n}\varphi_{\alpha mn}\exp\left(\mathrm{j}2\pi\frac{m}{L}x\right)\exp\left(\mathrm{j}2\pi\frac{n}{L}y\right)\right] \\ &= \sum_{m,n}\varphi_{\alpha mn}^{\mathrm{r}}\cos\left[\frac{2\pi}{L}(mx+ny)\right]-\sum_{m,n}\varphi_{\alpha mn}^{\mathrm{i}}\sin\left[\frac{2\pi}{L}(mx+ny)\right],\end{aligned} \tag{18}$$

where $\varphi_{\alpha mn}$, the Fourier series coefficients, are zero mean circular complex Gaussian random numbers and $L = N\Delta$ is the size of the discrete grid. Here, $\varphi_{\alpha mn}^{\mathrm{r}}$ and $\varphi_{\alpha mn}^{\mathrm{i}}$ are the real and imaginary parts of $\varphi_{\alpha mn}$, respectively.

Taking the autocorrelation of ϕ_α, making use of the assumption that $\varphi_{\alpha mn}$ are circular complex Gaussian random numbers, and simplifying yields

$$\left\langle \phi_\alpha(x_1,y_1)\phi_\alpha^*(x_2,y_2)\right\rangle = \sum_{m,n}\sum_{p,q}\left\langle \varphi_{\alpha mn}^{\mathrm{r}}\varphi_{\alpha pq}^{\mathrm{r}}\right\rangle\cos\left[\frac{2\pi}{L}(mx_1+ny_1-px_2-qy_2)\right]. \tag{19}$$

This expression must be equal to the autocorrelation of ϕ_α computed using Eqs. (16) and (17); therefore,

$$\begin{aligned}\left\langle \varphi_{\alpha mn}^{\mathrm{r}}\varphi_{\alpha pq}^{\mathrm{r}}\right\rangle &= \left\langle \varphi_{\alpha mn}^{\mathrm{i}}\varphi_{\alpha pq}^{\mathrm{i}}\right\rangle = \Phi_{\phi_\alpha\phi_\alpha}\left(\frac{m}{L},\frac{n}{L}\right)\delta_{mp}\delta_{nq}\frac{1}{L^2} \\ \left\langle\left(\varphi_{\alpha mn}^{\mathrm{r}}\right)^2\right\rangle &= \left\langle\left(\varphi_{\alpha mn}^{\mathrm{i}}\right)^2\right\rangle = \Phi_{\phi_\alpha\phi_\alpha}\left(\frac{m}{L},\frac{n}{L}\right)\frac{1}{L^2},\end{aligned} \tag{20}$$

where $\Phi_{\phi_\alpha\phi_\alpha}\left(f_x,f_y\right) = \sigma_{\phi_\alpha}^2\pi\ell_{\phi_\alpha\phi_\alpha}^2\exp\left[-\pi^2\ell_{\phi_\alpha\phi_\alpha}^2\left(f_x^2+f_y^2\right)\right]$ is the power spectral density of ϕ_α, $\left\langle\left(\varphi_{\alpha mn}^{\mathrm{r}}\right)^2\right\rangle$ and $\left\langle\left(\varphi_{\alpha mn}^{\mathrm{i}}\right)^2\right\rangle$ are the variances of the real and imaginary parts of the Fourier series coefficients $\varphi_{\alpha mn}$, and δ_{mp} and δ_{nq} are Kronecker deltas. The desired phase screen ϕ_α can be produced by using Eq. (18), namely,

#225412 - $15.00 USD Received 21 Oct 2014; revised 21 Nov 2014; accepted 25 Nov 2014; published 15 Dec 2014

$$\phi_\alpha[i,j] = \mathrm{Re}\left[\sum_{m,n} r_\alpha[m,n]\frac{\sigma_{\phi_\alpha}\sqrt{\pi}\ell_{\phi_\alpha\phi_\alpha}}{N\Delta}\exp\left\{-\frac{\pi^2\ell_{\phi_\alpha\phi_\alpha}^2}{2}\left[\left(\frac{m}{N\Delta}\right)^2+\left(\frac{n}{N\Delta}\right)^2\right]\right\}\right.$$
$$\left.\exp\left(\mathrm{j}\frac{2\pi}{N}mi\right)\exp\left(\mathrm{j}\frac{2\pi}{N}nj\right)\right], \tag{21}$$

where r_α is a matrix of zero mean circular complex Gaussian random numbers with the real and imaginary parts each having unit variance.

In order to generate correlated ϕ_x and ϕ_y, necessary to synthesize the "cross" terms of the CSD matrix, the cross-correlation of Eq. (21) must be computed:

$$\begin{aligned}\left\langle\phi_x[i,j]\phi_y[k,l]\right\rangle = \sum_{m,n}\sum_{p,q}&\frac{\sigma_{\phi_x}\sqrt{\pi}\ell_{\phi_x\phi_x}}{N\Delta}\exp\left\{-\frac{\pi^2\ell_{\phi_x\phi_x}^2}{2}\left[\left(\frac{m}{N\Delta}\right)^2+\left(\frac{n}{N\Delta}\right)^2\right]\right\}\\ &\frac{\sigma_{\phi_y}\sqrt{\pi}\ell_{\phi_y\phi_y}}{N\Delta}\exp\left\{-\frac{\pi^2\ell_{\phi_y\phi_y}^2}{2}\left[\left(\frac{p}{N\Delta}\right)^2+\left(\frac{q}{N\Delta}\right)^2\right]\right\}\\ &\left\langle\left\{r_x^{\mathrm{r}}[m,n]\cos\left(\frac{2\pi}{N}(mi+nj)\right)-r_x^{\mathrm{i}}[m,n]\sin\left(\frac{2\pi}{N}(mi+nj)\right)\right\}\right.\\ &\left.\left\{r_y^{\mathrm{r}}[p,q]\cos\left(\frac{2\pi}{N}(pk+ql)\right)-r_y^{\mathrm{i}}[p,q]\sin\left(\frac{2\pi}{N}(pk+ql)\right)\right\}\right\rangle,\end{aligned} \tag{22}$$

where r^{r} and r^{i} are the real and imaginary parts of r, respectively. Expanding the terms inside the angle brackets, letting

$$\begin{aligned}\left\langle r_x^{\mathrm{r}}[m,n]r_y^{\mathrm{r}}[p,q]\right\rangle = \left\langle r_x^{\mathrm{i}}[m,n]r_y^{\mathrm{i}}[p,q]\right\rangle &= \Gamma\delta_{mp}\delta_{nq}\\ \left\langle r_x^{\mathrm{r}}[m,n]r_y^{\mathrm{i}}[p,q]\right\rangle = \left\langle r_x^{\mathrm{i}}[m,n]r_y^{\mathrm{r}}[p,q]\right\rangle &= 0,\end{aligned} \tag{23}$$

where $0 \le \Gamma \le 1$ is a correlation coefficient, and simplifying yields

$$\left\langle\phi_x[i,j]\phi_y[k,l]\right\rangle = \sum_{m,n}\frac{\sigma_{\phi_x}\sigma_{\phi_y}\pi\ell_{\phi_x\phi_x}\ell_{\phi_y\phi_y}}{(N\Delta)^2}\frac{\Gamma}{2}\exp\left\{-\pi^2\left(\frac{\ell_{\phi_x\phi_x}^2+\ell_{\phi_y\phi_y}^2}{2}\right)\left[\left(\frac{m}{N\Delta}\right)^2+\left(\frac{n}{N\Delta}\right)^2\right]\right\}$$
$$\left\{\exp\left(\mathrm{j}\frac{2\pi}{N}m(i-k)\right)\exp\left(\mathrm{j}\frac{2\pi}{N}n(j-l)\right)+\exp\left(-\mathrm{j}\frac{2\pi}{N}m(i-k)\right)\exp\left(-\mathrm{j}\frac{2\pi}{N}n(j-l)\right)\right\}. \tag{24}$$

Note that the complex exponential terms in the braces are discrete inverse and forward Fourier transform kernels. The discrete function being transformed in Eq. (24), equivalent to the cross-power spectral density, is even in m and n; therefore, the forward and inverse Fourier transforms yield the same result. Applying these simplifications produces

$$\left\langle\phi_x[i,j]\phi_y[k,l]\right\rangle = \sum_{m,n}\sigma_{\phi_x}\sigma_{\phi_y}\pi\left(\Gamma\ell_{\phi_x\phi_x}\ell_{\phi_y\phi_y}\right)\exp\left\{-\pi^2\left(\frac{\ell_{\phi_x\phi_x}^2+\ell_{\phi_y\phi_y}^2}{2}\right)\left[\left(\frac{m}{N\Delta}\right)^2+\left(\frac{n}{N\Delta}\right)^2\right]\right\}$$
$$\exp\left(\mathrm{j}\frac{2\pi}{N}m(i-k)\right)\exp\left(\mathrm{j}\frac{2\pi}{N}n(j-l)\right)\frac{1}{(N\Delta)^2}. \tag{25}$$

#225412 - $15.00 USD Received 21 Oct 2014; revised 21 Nov 2014; accepted 25 Nov 2014; published 15 Dec 2014

By comparing the discrete function being transformed in Eq. (25) to the continuous cross-power spectral density function, i.e.,

$$\Phi_{\phi_x\phi_y}\left(f_x, f_y\right) = \sigma_{\phi_x}\sigma_{\phi_y}\pi\rho_{\phi_x\phi_y}\ell^2_{\phi_x\phi_y}\exp\left[-\pi^2\ell^2_{\phi_x\phi_y}\left(f_x^2 + f_y^2\right)\right], \tag{26}$$

one obtains the following relationships:

$$\begin{aligned}\ell_{\phi_x\phi_y} &= \sqrt{\frac{\Gamma\ell_{\phi_x\phi_x}\ell_{\phi_y\phi_y}}{\rho_{\phi_x\phi_y}}} = \sqrt{\frac{\ell^2_{\phi_x\phi_x} + \ell^2_{\phi_y\phi_y}}{2}} \\ \Gamma &= \frac{\rho_{\phi_x\phi_y}\left(\ell^2_{\phi_x\phi_x} + \ell^2_{\phi_y\phi_y}\right)}{2\ell_{\phi_x\phi_x}\ell_{\phi_y\phi_y}}.\end{aligned} \tag{27}$$

Using Eq. (9), the general relationships between the EGSM source parameters and the phase screen design parameters are found to be

$$\begin{aligned}\delta_{xx} &= \frac{1}{\sqrt{2}}\frac{\ell_{\phi_x\phi_x}}{\sigma_{\phi_x}} \\ \delta_{yy} &= \frac{1}{\sqrt{2}}\frac{\ell_{\phi_y\phi_y}}{\sigma_{\phi_y}} \\ \delta_{xy} &= \frac{1}{\sqrt{2}}\frac{\ell^2_{\phi_x\phi_x} + \ell^2_{\phi_y\phi_y}}{\sqrt{4\Gamma\sigma_{\phi_x}\sigma_{\phi_y}\ell_{\phi_x\phi_x}\ell_{\phi_y\phi_y}}} \\ \left|B_{xy}\right| &= \exp\left[-\frac{1}{2}\left(\sigma^2_{\phi_x} - \frac{4\Gamma\sigma_{\phi_x}\sigma_{\phi_y}\ell_{\phi_x\phi_x}\ell_{\phi_y\phi_y}}{\ell^2_{\phi_x\phi_x} + \ell^2_{\phi_y\phi_y}} + \sigma^2_{\phi_y}\right)\right].\end{aligned} \tag{28}$$

In the above equations, $\ell_{\phi_x\phi_x}$, $\ell_{\phi_y\phi_y} > 0$, σ_{ϕ_x}, $\sigma_{\phi_y} \geq \pi$, and $0 < \Gamma \leq 1$.

Equation (28) expresses the four desired EGSM source parameters in terms of five phase screen design parameters; thus, the system of nonlinear equations is undetermined. Upon closer inspection of Eq. (28), one notes that three of the four desired EGSM parameters can be chosen at will (recall that A_x, A_y, and $\angle B_{xy}$ can be chosen freely). The values of the three chosen parameters then set the value of the remaining one. This is most evident if one decides to choose the values of δ_{xx}, δ_{yy}, and δ_{xy}. The value of $\left|B_{xy}\right|$ is then set by the values of those other parameters. This is in contrast to previous EGSM synthesis research where δ_{xy} was a function of δ_{xx} and δ_{yy} [18–20].

While Eq. (28) could be inverted in the manner just outlined, the optimal solution is not guaranteed. Here, the optimal solution is defined as the phase screen design parameters that yield EGSM parameters "nearest to" the desired EGSM parameters. Thus, in this work, the optimal phase screen design parameters are found using constrained nonlinear optimization.

2.4. Generating complex screens (CS approach)

In this section, a method for synthesizing discretized T_x and T_y is shown. Because both amplitude and phase must be controlled, the CS approach is much better suited to research involving simulation. For ease of comparison, the same SLM specifications listed above are used in the simulation results presented in Section 3.

#225412 - $15.00 USD Received 21 Oct 2014; revised 21 Nov 2014; accepted 25 Nov 2014; published 15 Dec 2014

Like ϕ_α in the PS approach, the complex screen transmittances have zero mean and a Gaussian correlation function, i.e.,

$$\begin{aligned}\left\langle T_x(x,y)\right\rangle &= \left\langle T_y(x,y)\right\rangle = \left\langle T_\alpha(x,y)\right\rangle = 0\\ \left\langle T_\alpha(x_1,y_1)T_\alpha^*(x_2,y_2)\right\rangle &= \sigma_{T_\alpha}^2 \exp\left(-\frac{\left|\boldsymbol{\rho}_1-\boldsymbol{\rho}_2\right|^2}{\ell_{T_\alpha T_\alpha}^2}\right).\end{aligned} \tag{29}$$

Expanding T_α in a Fourier series yields

$$T_\alpha(x,y) = \sum_{m,n} \mathcal{T}_{\alpha mn} \exp\left(\mathrm{j}2\pi\frac{m}{L}x\right)\exp\left(\mathrm{j}2\pi\frac{n}{L}y\right), \tag{30}$$

where $\mathcal{T}_{\alpha mn}$, the Fourier series coefficients, are zero mean circular complex Gaussian random numbers and $L = N\Delta$ is, again, the size of the discrete grid. Taking the autocorrelation of T_α produces

$$\left\langle T_\alpha(x_1,y_1)T_\alpha^*(x_2,y_2)\right\rangle = \sum_{m,n}\sum_{p,q}\left\langle \mathcal{T}_{\alpha mn}\mathcal{T}_{\alpha pq}^*\right\rangle \exp\left[\mathrm{j}\frac{2\pi}{L}(mx_1-px_2)\right]\exp\left[\mathrm{j}\frac{2\pi}{L}(ny_1-qy_2)\right]. \tag{31}$$

Like in the PS approach, Eq. (31) can be shown to be equal to the autocorrelation of T_α, computed using similar Fourier transform relations as given in Eq. (16) and the expression given in Eq. (29). Performing the necessary analysis, one deduces that

$$\begin{aligned}\left\langle \mathcal{T}_{\alpha mn}\mathcal{T}_{\alpha pq}^*\right\rangle &= \Phi_{T_\alpha T_\alpha}\left(\frac{m}{L},\frac{n}{L}\right)\delta_{mp}\delta_{nq}\frac{1}{L^2}\\ \left\langle\left|\mathcal{T}_{\alpha mn}\right|^2\right\rangle &= \Phi_{T_\alpha T_\alpha}\left(\frac{m}{L},\frac{n}{L}\right)\frac{1}{L^2},\end{aligned} \tag{32}$$

where $\Phi_{T_\alpha T_\alpha}(f_x,f_y) = \sigma_{T_\alpha}^2\pi\ell_{T_\alpha T_\alpha}^2\exp\left[-\pi^2\ell_{T_\alpha T_\alpha}^2\left(f_x^2+f_y^2\right)\right]$ is the power spectral density of T_α and $\left\langle\left|\mathcal{T}_{\alpha mn}\right|^2\right\rangle$ is the variance of the Fourier series coefficients $\mathcal{T}_{\alpha mn}$. The complex amplitude screen T_α can be produced by using Eq. (30), i.e.,

$$\begin{aligned}T_\alpha[i,j] = \sum_{m,n} r_\alpha[m,n]\frac{\sigma_{T_\alpha}\sqrt{\pi/2}\ell_{T_\alpha T_\alpha}}{N\Delta}\exp\left\{-\frac{\pi^2\ell_{T_\alpha T_\alpha}^2}{2}\left[\left(\frac{m}{N\Delta}\right)^2+\left(\frac{n}{N\Delta}\right)^2\right]\right\}\\ \exp\left(\mathrm{j}\frac{2\pi}{N}mi\right)\exp\left(\mathrm{j}\frac{2\pi}{N}nj\right),\end{aligned} \tag{33}$$

where r_α is, again, a matrix of zero mean circular complex Gaussian random numbers with the real and imaginary parts each having unit variance.

In a manner completely analogous to the PS approach presented above, the cross-correlation of Eq. (33) must be computed. Using Eq. (23) and simplifying yields

#225412 - $15.00 USD Received 21 Oct 2014; revised 21 Nov 2014; accepted 25 Nov 2014; published 15 Dec 2014

$$\left\langle T_x[i,j]T_y^*[k,l]\right\rangle = \sum_{m,n}\sigma_{T_x}\sigma_{T_y}\pi\ell_{T_xT_x}\ell_{T_yT_y}\Gamma$$
$$\exp\left\{-\pi^2\left(\frac{\ell_{T_xT_x}^2+\ell_{T_yT_y}^2}{2}\right)\left[\left(\frac{m}{N\Delta}\right)^2+\left(\frac{n}{N\Delta}\right)^2\right]\right\} \tag{34}$$
$$\exp\left[\mathrm{j}\frac{2\pi}{N}m(i-k)\right]\exp\left[\mathrm{j}\frac{2\pi}{N}n(j-l)\right]\frac{1}{(N\Delta)^2}.$$

By comparing the discrete function being inverse Fourier transformed in Eq. (34) to the continuous cross-power spectral density function, i.e.,

$$\Phi_{T_xT_y}(f_x,f_y) = \sigma_{T_x}\sigma_{T_y}\pi\rho_{T_xT_y}\ell_{T_xT_y}^2\exp\left[-\pi^2\ell_{T_xT_y}^2\left(f_x^2+f_y^2\right)\right], \tag{35}$$

one obtains the following relationships:

$$\ell_{T_xT_y} = \sqrt{\frac{\Gamma\ell_{T_xT_x}\ell_{T_yT_y}}{\rho_{T_xT_y}}} = \sqrt{\frac{\ell_{T_xT_x}^2+\ell_{T_yT_y}^2}{2}}$$
$$\Gamma = \frac{\rho_{T_xT_y}\left(\ell_{T_xT_x}^2+\ell_{T_yT_y}^2\right)}{2\ell_{T_xT_x}\ell_{T_yT_y}}. \tag{36}$$

Using Eq. (15), the general relationships between the EGSM source parameters and the complex screen design parameters are

$$\delta_{xx} = \frac{\ell_{T_xT_x}}{\sqrt{2}}$$
$$\delta_{yy} = \frac{\ell_{T_yT_y}}{\sqrt{2}}$$
$$\delta_{xy} = \frac{1}{\sqrt{2}}\sqrt{\frac{\ell_{T_xT_x}^2+\ell_{T_yT_y}^2}{2}} \tag{37}$$
$$|B_{xy}| = \frac{2\Gamma\ell_{T_xT_x}\ell_{T_yT_y}}{\ell_{T_xT_x}^2+\ell_{T_yT_y}^2}.$$

In the above equations, $\ell_{T_xT_x}$, $\ell_{T_yT_y} > 0$ and $0 < \Gamma \le 1$.

It is clear from Eq. (37) that two of the three correlation function widths can be chosen freely (the third is set by the other two). One is generally free to choose the value of $|B_{xy}|$ subject to the constraint that $\Gamma \le 1$. The other EGSM source parameters, A_x, A_y, and $\angle B_{xy}$, can be chosen at will.

3. Validation

3.1 Simulation description

In this section, simulation results are presented to validate the PS and CS approaches described above. As stated previously, 512 points per side and a spacing of $15\,\mu$m were used to discretize the fields along paths 1 and 2 in Fig. 1. These numbers were chosen to match the BNS Model P512-0635 SLM. A wavelength of $\lambda = 632.8$ nm was assumed. Two different EGSM sources were simulated. The first was a linearly, partially polarized EGSM source

#225412 - $15.00 USD Received 21 Oct 2014; revised 21 Nov 2014; accepted 25 Nov 2014; published 15 Dec 2014

with the off-diagonal elements of the CSD matrix equal to zero. Since for this case $\sigma_x = \sigma_y$, the polarization state was uniform across the source plane [2]. The second was an elliptically partially polarized EGSM source with a fully-populated CSD matrix. Table 1 reports the desired, PS, and CS EGSM source parameters for both cases.

Table 1. EGSM Source Parameters

Case I ($W_{xy} = W_{yx} = 0$)

	A_x	A_y	$\angle B_{xy}$	σ_x (mm)	σ_y (mm)	δ_{xx} (mm)	δ_{yy} (mm)	δ_{xy} (mm)	$\lvert B_{xy} \rvert$
Desired	1.2	1	0	0.4286	0.4286	**0.1071**	**0.1429**	**0.1714**	**0**
PS	1.2	1	0	0.4286	0.4286	***0.1071***	***0.1429***	***0.1714***	***5.2 ‰ 10^{-11}***
CS	1.2	1	0	0.4286	0.4286	***0.1071***	***0.1429***	***0.1263***	***0***

Case II (Fully-Populated CSD Matrix)

	A_x	A_y	$\angle B_{xy}$	σ_x (mm)	σ_y (mm)	δ_{xx} (mm)	δ_{yy} (mm)	δ_{xy} (mm)	$\lvert B_{xy} \rvert$
Desired	1.3	1	$-\pi/6$	0.4286	0.3750	**0.1500**	**0.1607**	**0.1714**	**0.1500**
PS	1.3	1	$-\pi/6$	0.4286	0.3750	***0.1501***	***0.1608***	***0.1713***	***0.1500***
CS	1.3	1	$-\pi/6$	0.4286	0.3750	***0.1500***	***0.1607***	***0.1554***	***0.1500***

The screen parameters for the PS and CS approaches were determined by inverting Eqs. (28) and (37), respectively. For the CS approach, Eq. (37) is easily inverted. When the off-diagonal elements of the desired CSD matrix are zero (Case I), the CS approach can generate an EGSM source with the desired parameters (note that δ_{xy} is irrelevant in these cases). This is not guaranteed when the desired CSD matrix is fully populated (Case II), however.

For the PS approach, Eq. (28) is a coupled system of nonlinear equations and not easily inverted. Here, constrained nonlinear optimization was used to find the phase screen parameters such that

$$\arg\min_{\boldsymbol{x}\in\mathbb{R}} \sqrt{\left(\frac{\delta_{xx}^{\text{desired}}}{\delta_{xx}(\boldsymbol{x})}-1\right)^2+\left(\frac{\delta_{yy}^{\text{desired}}}{\delta_{yy}(\boldsymbol{x})}-1\right)^2+\left(\frac{\delta_{xy}^{\text{desired}}}{\delta_{xy}(\boldsymbol{x})}-1\right)^2+\left(\frac{\left|B_{xy}^{\text{desired}}\right|}{\left|B_{xy}(\boldsymbol{x})\right|}-1\right)^2}, \quad (38)$$

where $\boldsymbol{x}$ was a vector of the unknown phase screen parameters. The constraints on $\boldsymbol{x}$ included the conditions given in Eqs. (2) and (3) as well as positivity. In addition, to satisfy the "strongly scattering screen" requirement, i.e., the Gaussian approximation to the joint characteristic function [see Eq. (8)], $\sigma_{\phi_x}, \sigma_{\phi_y} \geq \pi$. Like in the CS approach, when the off-diagonal elements of the desired CSD matrix are zero (Case I), the PS approach can generate an EGSM source with the desired parameters. Again, this is not guaranteed when the desired CSD matrix is fully populated (Case II).

#225412 - $15.00 USD Received 21 Oct 2014; revised 21 Nov 2014; accepted 25 Nov 2014; published 15 Dec 2014

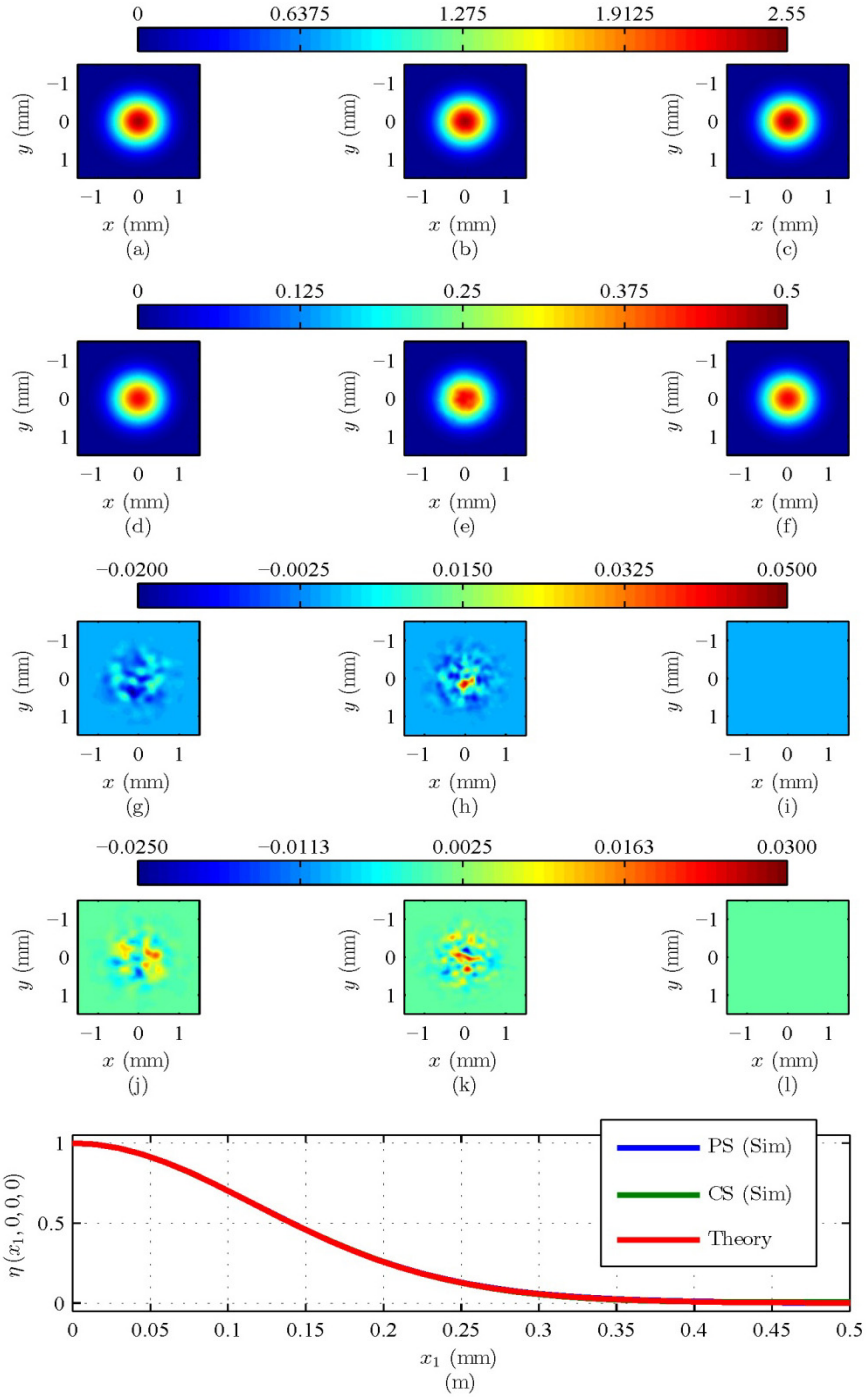

Fig. 2. Case I PS and CS simulation results versus theory. The rows are S_0, S_1, S_2, S_3, and η, respectively, while the columns are the PS, CS, and theory results, respectively. Each row of images is on the same color scale specified by the color bar in each row.

#225412 - $15.00 USD Received 21 Oct 2014; revised 21 Nov 2014; accepted 25 Nov 2014; published 15 Dec 2014

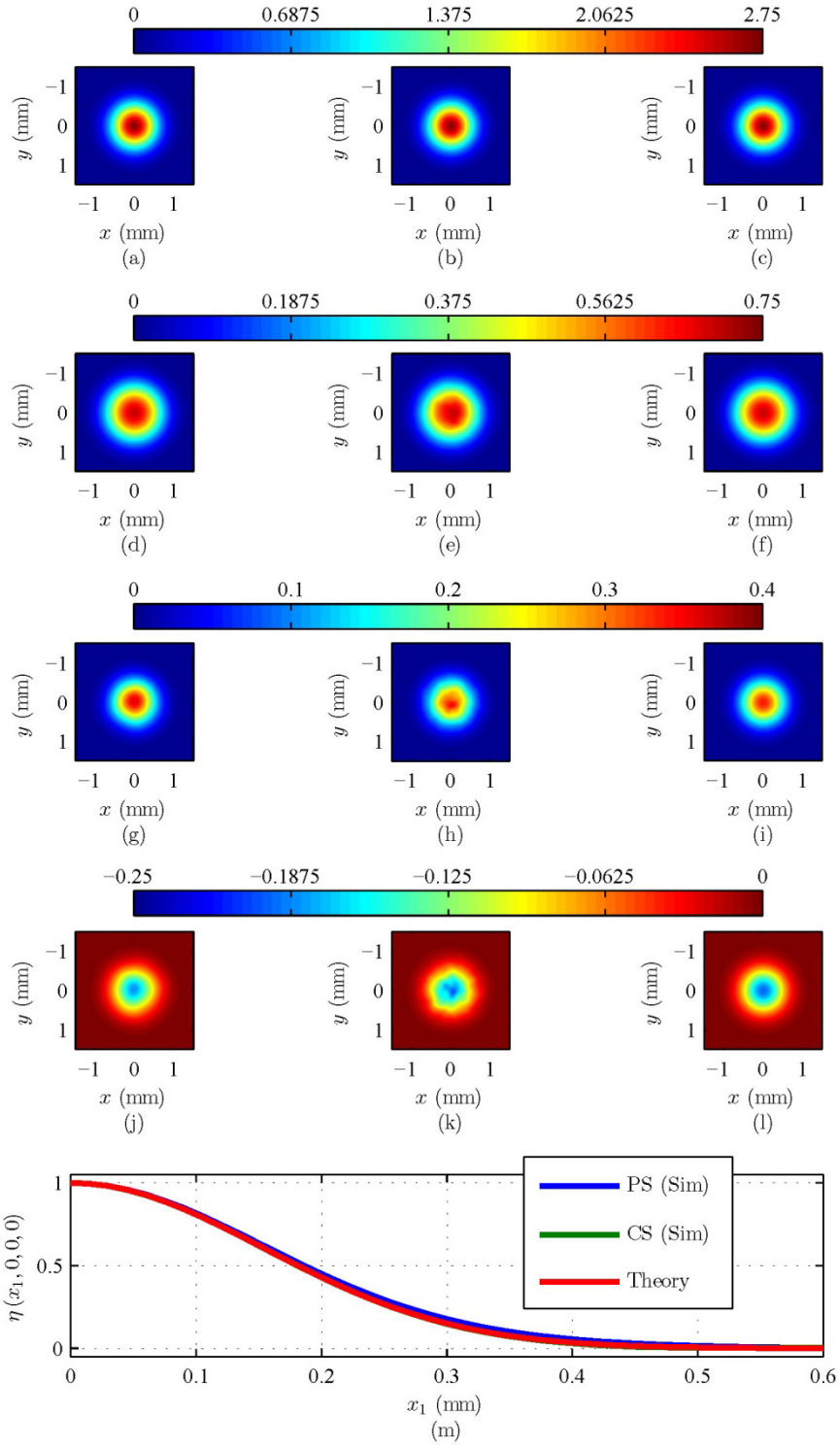

Fig. 3. Case II PS and CS simulation results versus theory. The rows are S_0, S_1, S_2, S_3, and η, respectively, while the columns are the PS, CS, and theory results, respectively. Each row of images is on the same color scale specified by the color bar in each row.

#225412 - $15.00 USD Received 21 Oct 2014; revised 21 Nov 2014; accepted 25 Nov 2014; published 15 Dec 2014

3.2 Simulation results

Figure 2 and Fig. 3 show the simulation results for Case I and II, respectively. The figures are organized such that the PS, CS, and theoretical results are along the columns—PS results are Figs. 2(a), 2(d), 2(g), 2(j) and Figs. 3(a), 3(d), 3(g), 3(j); CS results are Figs. 2(b), 2(e), 2(h), 2(k) and Figs. 3(b), 3(e), 3(h), 3(k) ; and theoretical results are Figs. 2(c), 2(f), 2(i), 2(l) and Figs. 3(c), 3(f), 3(i), 3(l) . Each row of images in Figs. 2 and 3 is a Stokes parameter— S_0 are Figs. 2(a)-2(c) and Figs. 3(a)-3(c); S_1 are Figs. 2(d)-2(f) and Figs. 3(d)-3(f); S_2 are Figs. 2(g)-2(i) and Figs. 3(g)-3(i); and S_3 are Figs. 2(j)-2(l) and Figs. 3(j)-3(l)—and on the same color scale specified by the color bar in each row. Lastly, the spectral degree of coherence η is shown in Figs. 2(m) and 3(m). The PS and CS statistics were computed at the simulated EGSM source plane (see Fig. 1) using the results of 20,000 simulations. The theoretical Stokes parameters and η are related to the CSD matrix elements by [27],

$$\begin{aligned} S_0(\boldsymbol{\rho}) &= W_{xx}(\boldsymbol{\rho},\boldsymbol{\rho}) + W_{yy}(\boldsymbol{\rho},\boldsymbol{\rho}) \\ S_1(\boldsymbol{\rho}) &= W_{xx}(\boldsymbol{\rho},\boldsymbol{\rho}) - W_{yy}(\boldsymbol{\rho},\boldsymbol{\rho}) \\ S_2(\boldsymbol{\rho}) &= W_{xy}(\boldsymbol{\rho},\boldsymbol{\rho}) + W_{yx}(\boldsymbol{\rho},\boldsymbol{\rho}) \\ S_3(\boldsymbol{\rho}) &= \mathrm{j}\left[W_{yx}(\boldsymbol{\rho},\boldsymbol{\rho}) - W_{xy}(\boldsymbol{\rho},\boldsymbol{\rho})\right] \\ \eta(\boldsymbol{\rho}_1,\boldsymbol{\rho}_2) = \eta(x_1,y_1,x_2,y_2) &= \frac{\mathrm{Tr}\,\mathbf{W}(\boldsymbol{\rho}_1,\boldsymbol{\rho}_2)}{\sqrt{\mathrm{Tr}\,\mathbf{W}(\boldsymbol{\rho}_1,\boldsymbol{\rho}_1)}\sqrt{\mathrm{Tr}\,\mathbf{W}(\boldsymbol{\rho}_2,\boldsymbol{\rho}_2)}}, \end{aligned} \tag{39}$$

where Tr is the trace of the CSD matrix $\mathbf{W}$ [10].

4. Conclusion

Two random screen methods, the PS and CS approaches, for generating EGSM sources were developed. The relationships between the desired source parameters and the random screen parameters were derived and discussed. For the CS approach, these relations were easily inverted. Eight of the nine desired EGSM source parameters could be produced exactly—any two of δ_{xx} , δ_{yy} , or δ_{xy} could be produced exactly (the remaining parameter's value is set by the values of the other two). The CS approach is well suited for simulation purposes; however, it is difficult to implement in the laboratory because field amplitude (in addition to phase) must be controlled. A major advantage of this method is its ability to easily simulate non-Gaussian electromagnetic Schell-model sources.

For the PS method, the relations between the desired EGSM source parameters and the screen parameters formed a system of coupled nonlinear equations which could not be analytically inverted. Constrained nonlinear optimization was used to find the best solution. In theory, all nine EGSM source parameters could be produced exactly because the nonlinear system was underdetermined, i.e., there are more screen parameters than desired EGSM source parameters. However, because of the complexity of the inverse problem, the optimal parameters were (generally) slightly different than the desired EGSM parameters. The PS approach is well suited for both simulation and laboratory experiments. Future work is needed to generalize this approach to non-Gaussian electromagnetic Schell-model sources.

Both the PS and CS approaches were tested through numerical wave optics simulations. The simulation results showed excellent agreement with published theory, thus validating the proposed approaches. Future work will include implementation of the approaches in the laboratory.

#225412 - $15.00 USD Received 21 Oct 2014; revised 21 Nov 2014; accepted 25 Nov 2014; published 15 Dec 2014

Acknowledgments

This research was supported in part by an appointment to the Postgraduate Research Participation Program at the Air Force Institute of Technology administered by the Oak Ridge Institute for Science and Education through an interagency agreement between the U.S. Department of Energy and AFIT.

O. Korotkova's research is supported by AFOSR (FA9550-12-1-0449) and ONR (N00189-12-T-0136).

D. Voelz's research is supported by the Air Force Office of Scientific Research (AFOSR) Multidisciplinary Research Program of the University Research Initiative (MURI) Grant FA9550-12-1-0449.

The views expressed in this paper are those of the authors and do not reflect the official policy or position of the U.S. Air Force, the Department of Defense, or the U.S. Government.

#225412 - $15.00 USD Received 21 Oct 2014; revised 21 Nov 2014; accepted 25 Nov 2014; published 15 Dec 2014